Spin Electronics

Comparison of Synthetic Antiferromagnets and Hard Ferromagnets as Reference Layer in Magnetic Tunnel Junctions With Perpendicular Magnetic Anisotropy

S. Bandiera[1], R. C. Sousa[1], Y. Dahmane[1], C. Ducruet[2], C. Portemont[2], V. Baltz[1], S. Auffret[1], I. L. Prejbeanu[1], and B. Dieny[1]*

[1] SPINTEC, UMR 8191 CEA/CNRS/UJF/Grenoble-INP//INAC, 38054 Grenoble, France
[2] Crocus Technology, 38025 Grenoble, France
*Senior Member, IEEE

Abstract—In magnetic tunnel junctions (MTJ), synthetic antiferromagnets (SAF) are usually used as reference layer to minimize dipolar interactions induced between this layer and the free layer (FL). We show here that the use of SAF allows us to reduce the asymmetry of the FL reversal due to stray fields in nanosized MTJs with perpendicular magnetic anisotropy.

I. INTRODUCTION

Magnetic tunnel junctions (MTJs) with perpendicular magnetic anisotropy (PMA) attract much interest since they allow to scale down the dimension of spintronic devices to the latest technological node (<45 nm), while keeping a sufficient thermal stability ($E/k_B T > 60$) and lowering the current density needed to switch the free layer (FL) by spin transfer torque [Mangin 2006]. It is also pointed out that circular pillars can be used instead of elliptical ones in the case of MTJs with PMA (p-MTJs), since shape anisotropy is not required for stability. This allows simplifying the fabrication process and gives the maximum areal bit density. Currently, p-MTJs use a wide variety of perpendicular materials such as Co/Pt [Carvello 2008] or CoFe/Pd [Mizunuma 2009] multilayers, $L1_0$FePt ordered alloys [Yoshikawa 2008], rare earth elements-transition metal (RE-TM) ferrimagnets [Nakayama 2008] or Pt/Co/oxide stacks [Nistor 2009]. In these systems, the reference layer consists of a single hard magnetic layer. However, except for the case of compensated RE-TM ferrimagnets, dipolar interaction between the two magnetic electrodes results in a highly asymmetrical reversal of the FL with respect to the applied field or to the current density. Moreover, if the induced shift of the loop (H_{coupl}) is greater than the FL coercive field (H_C), only one resistance state remains stable at zero field, which is not suitable for applications. For in-plane MTJ, this problem has been solved by replacing the pinned layer by a synthetic antiferromagnet (SAF) consisting of two ferromagnetic layers antiferromagnetically coupled through a nonmagnetic spacer layer (such as Ru) by the Ruderman–Kittel–Kasuya–Yosida coupling (J_{Ru}) [Parkin 1990]. In this system, when the antiferromagnetic configuration is stabilized because of the well-chosen Ru layer thickness, stray fields are considerably decreased [Leal 1998] and the shift of the FL hysteresis loop is greatly reduced. In the case of systems with PMA, such compensation has been previously studied for the purpose of multilevel recording [Baltz 2007, 2009]. In this letter, we investigate the effects of these stray fields in the context of MTJs and compare two types of p-MTJs: the first one using a single hard reference layer (HL), the other one using a perpendicular SAF. We find that SAF structures are highly suitable for magnetoresistive random access memories (MRAM) cells with PMA, especially when the diameter of the cells (Φ) is scaled down.

II. EXPERIMENTAL DETAILS

The two studied MTJ stacks are: HL/Al0.6+NatOx/FL (referred as HL-MTJ) and SAF/Al0.6+NatOx/FL (referred as SAF-MTJ). HL consists of Ta3/Pt30/(Co0.5/Pt0.4)5/Co0.5/CoFeB1, SAF of Ta3/Pt30/(Co0.5/Pt0.4)5/Co0.5/Ru0.85/(Co0.5/Pt0.4)3/Co0.5/CoFeB1, and FL of CoFe0.6/(Pt1.8/Co0.6)2/Pt2 (thickness in nm). The layers were deposited by dc magnetron sputtering onto a 100-mm diameter thermally oxidized silicon wafer with a base pressure of 8×10^{-8} mbar. The alumina tunnel barrier was obtained by a 5 min natural oxidation of the metallic aluminium layer under 160-mbar oxygen pressure. Samples were annealed at 250°C for 10 min. We patterned 140- and 540-nm diameter circular pillars through e-beam lithography and ion beam etching. Magnetic hysteresis loops were measured on unpatterned samples by extraordinary Hall effect (EHE) and vibrating sample magnetometer (VSM). Anisotropy fields (H_K) were measured by applying the magnetic field in the hard axis direction, i.e., in the plane of the magnetic layers. Electrical properties were first investigated by current in-plane tunneling (CIPT) measurements on unpatterned samples [Worledge 2003]. Resistance hysteresis loops were measured by two probes in a current perpendicular to the plane (CPP) configuration at 0.1 V bias on the nanosized pillars. We measured the resistance loops of ten pillars and calculated the mean coercive (m_{Hc}) and coupling fields (m_{Hcoupl}), as well as their standard deviation (σ_{Hc} and σ_{Hcoupl}) to take into account the properties distribution among the pillars.
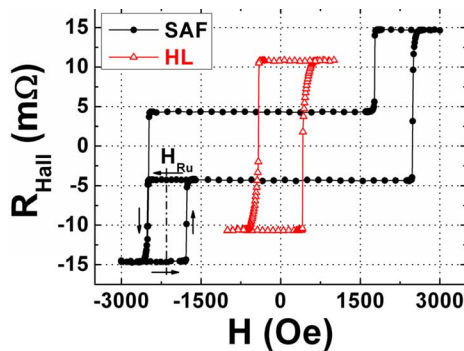
Fig. 1. Hysteresis loops measured by EHE for HL (red open triangles) and SAF (black filled circles) on unpatterned samples.

III. RESULTS AND DISCUSSION

The magnetic properties of SAF and HL have been first investigated on unpatterned samples by VSM and EHE. VSM measurements indicate that both magnetizations of SAF have a saturation magnetization of $M_S = 1200 \pm 50$ emu·cm^{-3}. The two moments are compensated, the macroscopic magnetization of SAF is equal to zero without applied field. The saturation magnetization of HL is also $M_S = 1200 \pm 50$ emu·cm^{-3}. Hysteresis loops measured by EHE are shown in Fig. 1. All magnetizations are perfectly aligned along the thin film plane normal. However, SAF presents much higher reversal fields. Such behavior can be explained by the different nucleation process in antiferromagnetically coupled perpendicular layers [Hellwig 2003]. The SAF presents two magnetic contributions: the jump at 2500 Oe corresponds to the bottom (Co/Pt) multilayer reversal, and the minor loop denoted by the black arrows in Fig. 1 corresponds to the top (Co/Pt)/CoFeB layers reversal. By measuring the shift H_{Ru} of the loop of the softest magnetic layer in SAF, we can deduce that $J_{Ru} = H_{Ru} t M_S = 0.8$ erg·cm^{-2} here. H_{Ru} is thus much larger than the coercive field of the minor loop, so that the antiferromagnetic configuration is the only stable one in zero field. EHE measurements show different level of resistance at zero field for SAF, whereas VSM measurements showed that both magnetizations where equal. The difference of Hall resistances contributions for the two magnetizations can be explained by the dependence in such systems of the skew scattering and quantum side jump factors on the composition of the magnetic layer and of its adjacent layers, as well as its thickness [Canedy 1997]. The Hall coefficient of the thick CoFeB layer is thus lower than the Co ones. The measurement of anisotropy fields indicates that the effective anisotropy is 4.6×10^6 erg·cm^{-3} for HL, 6×10^6 erg·cm^{-3} for the bottom SAF layer, and 3.6×10^6 erg·cm^{-3} for the top SAF layer. For a 90-nm-diameter cell, these correspond to $2820 k_B T$ for HL and $4400 k_B T$ for SAF. Such a high stability can be explained by the high PMA induced at the Co/Pt and CoFeB/AlOx interfaces [Nistor 2009].

For unpatterned samples, when the FL is added on top of the barrier, we obtain a complete p-MTJ. After annealing, the FL (Co/Pt) multilayer remains perpendicular to plane. The FL minor hysteresis loop is shifted by 40 Oe in a direction indicat-
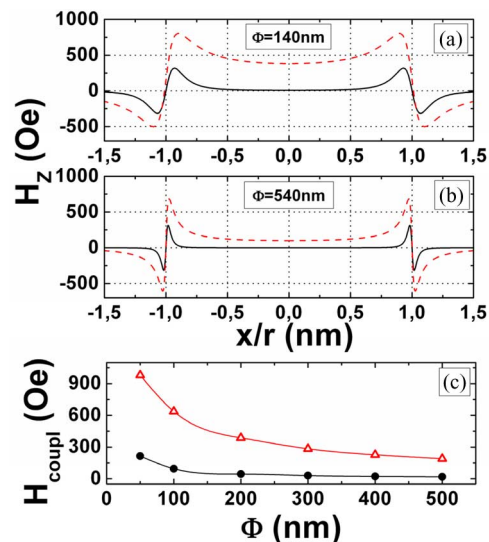

Fig. 2. (a) and (b) Calculation of stray fields Hz of SAF (black continuous line) and HL (red dashed line) along the lateral normalized dimension x/r, on (a) 140 nm and (b) 540 nm diameter pillars. (c) Calculation of mean stray fields H_{coupl} of SAF (filled black circles) and HL (opened red triangles) as a function of the pillar diameter Φ.

ing antiferromagnetic coupling across the alumina barrier. This coupling of 40 Oe is probably due to magnetostatic coupling induced by roughness [Moritz 2004], since AlO$_x$ is amorphous and pinholes would induce a ferromagnetic interlayer coupling. The magnetic anisotropy of this FL electrode is 2.6×10^5 erg·cm^{-3}, which is much smaller than the PMA of bottom electrodes (HL and SAF), due to poor growth conditions on the oxide, and the lack of (111) texture. Nevertheless, this corresponds to $95 k_B T$ for a 90-nm-diameter cell, which fulfils the stability condition for the 90-nm technological node. CIPT measurements indicate that this junction presents a TMR ratio of 6% and a resistance–area (RA) product of 21 Ω·μm^2. Such a low TMR ratio is probably due to small thickness of the top magnetic electrode and the absence of a reasonably long annealing [Sousa 1998], which would greatly improve barrier/magnetic layers interfaces. Moreover, it is probable that the Pt atoms diffuse to the barrier, enhancing nonspin-dependent tunneling conduction.

Fig. 2(a) and (b) shows calculation of the perpendicular to plane component of the stray fields (H$_z$) in a middle section of FL along the normalized lateral dimension x/r, r being the radius of the pillar, using a simple macrospin model that considers facing charged surfaces [Hubert 1998]. Both cases of HL and SAF have been investigated for different pillar diameters, assuming that all magnetic layers of HL and SAF have perfectly rigid perpendicularly oriented moments. Magnetization of each magnetic layer (Co or CoFeB) has been taken equal to 1200 emu·cm^{-3}, following VSM measurements. These calculations show that stray fields are greatly reduced when HL is replaced by the compensated SAF, due to its reduced effective magnetization. However, since the center of the two magnetic layers of SAF does not coincide, it cannot be cancelled everywhere, edges presenting higher fields due to the higher contribution given essentially by the closest layers.
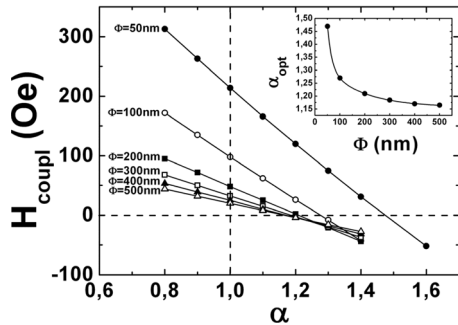
Fig. 3. Calculated dependence of the mean stray field H_{coupl} as a function of the magnetic moment ratio α. Inset: optimal ratio α_{opt}, i.e., for $H_{coupl} = 0$, as a function of Φ.

Fig. 3 shows the evolution of the calculated mean stray field $H_{coupl} = \int H_z(x, y)dxdy/(\pi r^2)$ for different dot diameters as a function of the ratio $\alpha = m_2/m_1$, m_1, and m_2 being, respectively, the magnetic moments of the top (Co/Pt)/CoFeB and the bottom (Co/Pt) multilayer. In this study, we only changed the number of repeats in the bottom (Co/Pt) multilayer in order to increase the contribution of this layer. For α equal to 1 (vertical dotted line), we have a perfectly compensated SAF giving the increased dipolar interaction when reducing the diameter of the pillar, as shown in Fig. 2(c). Fig. 3 (inset) gives the optimal ratio α_{opt} at which H_{coupl} is 0 (horizontal dotted line) as a function of the diameter. It is noticeable that when the diameter of the pillar decreases, the slope of $H_{coupl}(\alpha)$ increases, which means that the optimization becomes more sensitive to deviations from the perfect ratio. In summary, contributions of both layers have to be adjusted for each diameter to minimize dipolar interaction, by varying the magnetic layers thickness and/or the number of repeats of the (Co/Pt) multilayers on both sides of the Ru spacer.

Patterned samples show resistance hysteresis loops exhibiting TMR ratio varying from 0.5% to 6% and RA products varying from 10 to 28 $\Omega \cdot \mu m^2$. Optimal TMR ratios are obtained along with the nominal RA product of 21 $\Omega \cdot \mu m^2$. The spread of electrical properties from the CIPT measurements are essentially due to fabrications issues. No significant TMR or RA difference can be observed between HL-MTJ and SAF-MTJ junctions in terms of electrical properties. Fig. 4 presents hysteresis loops measured on one pillar of HL-MTJ and SAF-MTJ. It shows several steps on the 540-nm diameter pillars, probably due to the nonuniform reversal of the different magnetic grains of the FL, edge roughness on the dot or pinning and depinning of domain walls on defects in the pillar. Reducing the diameter to 140 nm makes the steps of FL reversal disappear, indicating a more coherent magnetization switching within individual pillars. However, the pillar to pillar fluctuations in H_C are larger in the smaller pillars due to a reduced number of grains and defects per pillar, as can be seen from the larger σ_{Hc} values on Table 1. The increase of σ_{Hc} when using a SAF reference layer for the 140-nm diameter pillars instead of single hard layer seems to be mainly due to fabrication reproducibility issues and should not be a problem when an optimized process for this kind of stacks will be achieved.
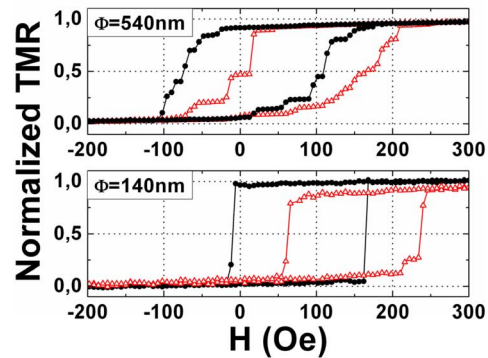

Fig. 4. Hysteresis resistance loops of the FL of HL-MTJ (red opened triangles) and SAF-MTJ (black filled circles) measured by CPP on patterned pillars.

Table 1. Summary of mean coupling and coercive fields along with their standard deviation measured on ten 140 and 540 nm pillars.

type	Φ	m_{Hcoupl}	σ_{Hcoupl}	m_{Hc}	σ_{Hc}
HL	140 nm	170 Oe	12 Oe	85 Oe	16 Oe
SAF	140 nm	80 Oe	17 Oe	95 Oe	26 Oe
HL	540 nm	100 Oe	14 Oe	90 Oe	11 Oe
SAF	540 nm	5 Oe	7 Oe	70 Oe	9 Oe

In these pillars, H_{coupl} contains different contributions: Néel coupling, pinholes, and stray field effects. Even if these different contributions cannot be separated in the present measurements, only the dipolar interactions should vary by changing the pillar size. The average of Néel and pinhole coupling can be estimated to be 40 Oe, as measured on the unpatterned sample. Nevertheless, the influence of the SAF is clearly seen on these loops: SAF-MTJ presents smaller shifts than HL-MTJ at the same diameter. Without SAF, only the parallel state remains stable at zero field for the smaller dots, whereas H_{coupl} is lower than H_C in SAF-MTJ. We can verify that stray fields greatly depend on the size of the MTJ, as predicted by calculations. Table 1 shows that 140 nm pillars of SAF-MTJ present a coupling field of 80 Oe since $\alpha = 1$ is not the optimal ratio for this diameter (calculations give $\alpha_{opt} = 1.23$), whereas it is only 5 Oe for the 540-nm diameter pillars in which $\alpha_{opt} = 1.16$, closer to the experimental one. The shift of the hysteresis loops of HL-MTJ is also increased up to 170 Oe for this diameter, significantly larger than in SAF-MTJ. However, the model does not fit our experimental data well, particularly for the smaller dots of HL-MTJ, which should present much higher H_{coupl}. This could be attributed to several factors, which are not taken into account in the model: possible oxidation of the sidewalls during the etching, which can decrease the magnetic moments [Yoshikawa 2006], geometrical imperfections of the dots, roughness, defects, and other inhomogeneities.

IV. CONCLUSION

In this letter, we showed that SAF-based reference layers are of great interest in p-MTJs. The SAF increases the reversal field of the hard layer, leading to an improved thermal stability and can minimize dipolar interactions between storage and

reference layers when magnetic moments are well adjusted. The reduction of stray fields is accompanied by a great reduction of the shift of the FL in patterned samples. This is essential in MRAM applications where two resistance states are required at zero field. However, stray fields cannot be cancelled everywhere across the FL surface, which implies that SAF parameters have to be designed for each pillar size in order to minimize the mean stray field.

Such structures can be used in combination with MgO tunnel barrier and Fe or CoFe insertions [Mizunuma 2009] at the barrier interfaces in order to fulfill TMR ratio requirements for high-density MRAMs.

ACKNOWLEDGMENT

REFERENCES

Baltz V, Bollero A, Rodmacq B, Dieny B, Jamet J-P, Ferré J (2007), "Multilevel magnetic nanodot arrays with out-of-plane anisotropy: The role of intra-dot magnetostatic coupling," *Eur. Phys. J.: Appl. Phys.*, vol. 39, pp. 33–38, doi: 10.1051/epjap:2007107.

Baltz V, Rodmacq B, Bollero A, Ferré J, Landis S, Dieny B (2009), "Balancing interlayer dipolar interactions in multilevel patterned medai with out-of-plane anisotropy," *Appl. Phys. Lett.*, vol. 94, 052503, doi: 10.1063/1.3078523.

Canedy C L, Li X W, Xiao G (1997), "Extraordinary Hall effect in (111) and (100)-oriented Co/Pt superlattices," *J. Appl. Phys.*, vol. 81, pp. 5367–5369, doi: 10.1063/1.364599.

Carvello B, Ducruet C, Rodmacq B, Auffret S, Gautier E, Gaudin G, Dieny B (2008), "Sizable room-temperature magnetoresistance in cobalt based magnetic tunnel junctions with out-of-plane anisotropy," *Appl. Phys. Lett.*, vol. 92, 102508, doi: 10.1063/1.2894198.

Hellwig O, Kirk T L, Kortright J B, Berger A, Fullertone E E (2003), "A new phase diagram for layered antiferromagnetic films," *Nature Mater.*, vol. 2, pp. 112–116, doi: 10.1038/nmat806.

Hubert A, Schäfer R (1998) *Magnetic Domains*. Berlin, Germany: Springer.

Leal J L, Kryder M H (1998), "Spin valves exchanges biased by Co/Ru/Co synthetic antiferromagnets," *J. Appl. Phys.*, vol. 83, pp. 3720–3723, doi: 0.1063/1.366597.

Mangin S, Ravelosona D, Katine J A, Carey M J, Terris B D, Fullertone E E (2006), "Current-inducedmagnetization reversal in nanopillars with perpendicular anisotropy," *Nature Mater.*, vol. 5, pp. 210–215, doi: 10.1038/nmat1595.

Mizunuma K, Ikeda S, Park J H, Yamamoto H, Gan H, Miuar K (2009), "MgO barrier-perpendicular magnetic tunnel junctions with CoFe/Pd multilayers and ferromagnetic insertion layers," *Appl. Phys. Lett.*, vol. 95, 232516, doi: 10.1063/1.3265740.

Moritz J, Garcia F, Toussaint J-C, Dieny B, Nozière J-P (2004), "Orange peel coupling in multilayers with perpendicular magnetic anisotropy: application to (Co/Pt)-based exchange-biased spin-valves," *Europhys. Lett.*, vol. 65, pp. 33–38, doi: 10.1209/epl/i2003-10063-9.

Nakayama M, Kai T, Shimomura M, Amano M, Kitagawa E, Nagase T (2008), "Spin transfer switching in TbCoFe/CoFeB/MgO/CoFeB/TbCoFe magnetic tunnel junctions with perpendicular magnetic anisotropy," *J. Appl. Phys.*, vol. 103, 07A710, doi: 10.1063/1.2838335.

Nistor L E, Rodmacq B, Auffret S, Bieny B (2009), "Pt/Co/oxide and oxide/Co/Pt electrodes for perpendicular magnetic tunnel junctions," *Appl. Phys. Lett.*, vol. 94, 012512, doi: 10.1063/1.3064162.

Parkin S S P, More N, Roche K P (1990), "Oscillations in exchange coupling and magnetoresistance in metallic superlattice structures—Co/Ru, Co/Cr, and Fe/Cr," *Phys. Rev. Lett.*, vol. 64, pp. 2304–2307, doi: 10.1103/PhysRevLett.64.2304.

Sousa R C, Sun J J, Soares V, Freitas P P, Kling A, da Silva M (1998), "Large tunneling magnetoresistance enhancement by thermal anneal," *Appl. Phys. Lett.*, vol. 73, pp. 3288–3290, doi: 10.1063/1.122747.

Worledge D C, Trouilloud P L (2003), "Magnetoresistance measurement of unpatterned magnetic tunnel junction wafers by current-in-plane tunneling," *Appl. Phys. Lett.*, vol. 83, pp. 84–86, doi: 10.1063/1.1590740.

Yoshikawa M, Kitagawa E, Nagase T, Daibou T, Nagamine M, Nishiyama K (2008), "Tunnel Magnetoresistance Over 100% in MgO-Based Magnetic Tunnel Junction Films With Perpendicular Magnetic $L1_0$-FePt Electrodes," *IEEE Trans. Magn.*, vol. 44, pp. 2573–2576, doi: 10.1109/TMAG.2008.2003059.

Yoshikawa M, Kitagawa E, Takahashi S, Kai T, Amano M, Shimomura N (2006), "Reduction of switching field distributions by edge oxidization of submicron magnetoresistive tunneling junction cells for high-density magnetoresistive random access memories," *J. Appl. Phys.*, vol. 99, 08R702, doi: 10.1063/1.2165138.